Unified description of fusion and multinucleon transfer processes within the dinuclear system model

Long Zhu* and Jun Su
Sino-French Institute of Nuclear Engineering and Technology, Sun Yat-sen University, Zhuhai 519082, China

(Received 5 June 2021; accepted 27 September 2021; published 7 October 2021)

To compare fusion-evaporation (FE) and multinucleon transfer (MNT) approaches and make more reliable predictions for producing superheavy nuclei, the unified description of FE and MNT processes is performed in the reaction ^{48}Ca + ^{238}U within the (DNS) model. We extend the fusion concept in the DNS model based on the deformation degree of freedom. Our calculations support the experimental result [Nishio *et al.*, Phys. Rev. C **77**, 064607 (2008)] that compact configuration enhances the fusion probability. The experimental production cross sections of isotopes in FE and MNT processes can be simultaneously reproduced. By comparing the production cross sections in the MNT reaction ^{238}U + ^{248}Cm with the FE reactions ^{48}Ca + ^{238}U and ^{54}Cr + ^{248}Cm, we find that the FE process shows great advantages of cross sections for producing Cn isotopes and is the only approach that could produce superheavy elements beyond oganesson.

DOI: 10.1103/PhysRevC.104.044606

I. INTRODUCTION

The heavy-ion collisions around the Coulomb barrier have attracted a lot of attention in the past decades, especially the fusion-evaporation (FE) process for synthesizing the superheavy nuclei (SHN) [1] and the multinucleon transfer (MNT) process for investigating the equilibration mechanism in quantum many-body systems [2] and the production of exotic nuclei as well as SHN [3–6].

The main characteristic for the formation of the compound nucleus (CN) is full equilibration. The CN forgets the information in the entrance channel. In the MNT process, several nucleons are transferred from one nucleus to another with dissipation of incident energy and only partial statistical equilibrium can reach [2]. The fusion probability for producing SHN is extremely small. With increase of Coulomb repulsion, the CN formation probabilities decreases strongly. The dominant events end with separation of two fragments after a short contact time in MNT approach.

The elements with $Z = 102$–118 were synthesized in the approaches of the cold fusion reactions based on the ^{208}Pb and ^{209}Bi targets [7,8] and the ^{48}Ca-induced hot fusion reactions [9–15]. In recent years, the projectiles of ^{50}Ti-, ^{51}V-, ^{54}Cr-, ^{58}Fe-, and ^{64}Ni-induced hot fusion reactions have been investigated and proposed to synthesize the elements beyond oganesson [16–27]. And the search for the new elements $Z = 119$ and 120 will be carried out in several laboratories in the short term. On the other hand, the MNT process was demonstrated as one promising approach for producing neutron-rich isotopes around $N = 126$ [28,29] as well as one alternative approach for producing SHN [30,31], especially neutron-rich SHN.

Inspired by intriguing questions of partly fundamental character and abundant experimental data, many approaches have been used to investigate the mechanism of the FE reaction for synthesizing SHN [20,23,32–43]. Also, in recent years, due to the great potential for producing neutron-rich isotopes, several theoretical models were developed to explore the mechanism of the MNT process [44–54]. Among these approaches, the dinuclear system (DNS) model has been widely used in studying the mechanism of the synthesis of SHN in FE reactions [55–60] and the MNT process for producing exotic nuclei far from the stability line and SHN [61–70]. However, few works within the DNS model showed a unified description of the both FE and MNT processes. Actually, to compare the FE and MNT processes and make the reliable predictions for producing SHN, a unified description of the two approaches is indispensable.

In this work, we obtain a unified description of the FE and MNT processes based on the code of DNS-SYSU and compare the two approaches for producing SHN, including the element $Z = 120$. The article is organized as follows: In Sec. II, we describe the theoretical method in detail. The results and discussion are presented in Sec. III. Finally, we summarize the main results in Sec. IV.

II. THEORETICAL METHOD

The cross section for the production of nuclei with proton number Z_1^f and neutron number N_1^f in heavy-ion collisions can be written as

$$\sigma\left(Z_1^f, N_1^f, E_{\mathrm{c.m.}}\right) = \frac{\pi\hbar^2}{2\mu E_{\mathrm{c.m.}}} \sum_{J=0}^{J_{\max}} (2J+1) T_{\mathrm{cap}}(J, E_{\mathrm{c.m.}}) \times \sum_{\beta_2} P(Z_1, N_1, \beta_2, J, E_{\mathrm{c.m.}}, t = \tau_{\mathrm{int}}) W(Z_1, N_1, J, E^*). \quad (1)$$

*zhulong@mail.sysu.edu.cn

Here, T is the transmission probability, P is the formation probability of primary fragments, including the formation probability of compound nucleus, W is the deexcitation probability of primary excited fragment (Z_1, N_1) in specific channels to form the objective nucleus $(Z_1^{\rm f}, N_1^{\rm f})$, and $\tau_{\rm int}$ is the interaction time calculated with the deflection function [71,72].

A. Capture probability

The transmission probability is calculated by using the Hill-Wheeler formula in combination with the barrier distribution function, which can be written as

$$T_{\rm cap}(J, E_{\rm c.m.}) = \int \frac{f(B)dB}{1+\exp\left\{-\frac{2\pi}{\hbar\omega(J)}\left[E_{\rm c.m.} - B - \frac{\hbar^2}{2\mu R_B^2(J)}J(J+1)\right]\right\}}, \quad (2)$$

where $\hbar\omega(J) = \hbar(-\frac{1}{\mu}\frac{\partial^2 V}{\partial r^2})^{1/2}|_{R=R_B}$ is the width of the parabolic Coulomb barrier at the position $R_B(J)$. The enhancement of the subbarrier capture cross section can be attributed to the coupling between the relative motion of the two nuclei and other degrees of freedom and couplings to positive Q-value neutron transfer channels. These couplings lead to a distribution of barriers $f(B)$ rather than a single barrier [73].

B. Diffusion process

1. The master equation

In heavy-ion collisions near the Coulomb barrier, the primary fragment distribution probability can be obtained by using the master equation, which can be written as [74]

$$\begin{aligned}\frac{dP(Z_1, N_1, \beta_2, J, t)}{dt} &= \sum_{Z_1'} W_{Z_1,N_1,\beta_2;Z_1',N_1,\beta_2}(t)\left[d_{Z_1,N_1,\beta_2}P(Z_1', N_1, \beta_2, J, t) - d_{Z_1',N_1,\beta_2}P(Z_1, N_1, \beta_2, J, t)\right] \\ &+ \sum_{N_1'} W_{Z_1,N_1,\beta_2;Z_1,N_1',\beta_2}(t)\left[d_{Z_1,N_1,\beta_2}P(Z_1, N_1', \beta_2, J, t) - d_{Z_1,N_1',\beta_2}P(Z_1, N_1, \beta_2, J, t)\right] \\ &+ \sum_{\beta_2'} W_{Z_1,N_1,\beta_2;Z_1,N_1,\beta_2'}(t)\left[d_{Z_1,N_1,\beta_2}P(Z_1, N_1, \beta_2', J, t) - d_{Z_1,N_1,\beta_2'}P(Z_1, N_1, \beta_2, J, t)\right]. \end{aligned} \quad (3)$$

Here, $P(Z_1, N_1, \beta_2, J, t)$ is the distribution probability for fragment 1 with proton number Z_1 and neutron number N_1 at time t. β_2 is related to the dynamical deformation parameter of the collision partners. J is the entrance angular momentum. $\delta\beta_2^1 + \delta\beta_2^2 = 2\beta_2$, $C_1\delta\beta_2^1 = C_2\delta\beta_2^2$. $\delta\beta_2^1$ and $\delta\beta_2^2$ are the dynamical quadrupole deformations of fragment 1 [projectile-like fragment (PLF)] and fragment 2 [target-like fragment (TLF)], respectively. C_1 and C_2 are the liquid drop model stiffness parameters of the fragments [75]. $W_{Z_1,N_1,\beta_2;Z_1',N_1,\beta_2}$ denotes the mean transition probability from the channel (Z_1, N_1, β_2) to (Z_1', N_1, β_2), which is similar to N_1 and β_2. d_{Z_1,N_1,β_2} is the microscopic dimension (the number of channels) corresponding to the macroscopic state (Z_1, N_1, β_2) [76]. For the degrees of freedom of charge and neutron number, the sum is taken over all possible proton and neutron numbers that fragment 1 may take, but only one nucleon transfer is considered in the model $(Z_1' = Z_1 \pm 1; N_1' = N_1 \pm 1)$. For β_2, we take the range of -0.5–0.5. The evolution step length is 0.01. The transition probability is related to the local excitation energy [74,77].

2. Potential-energy surface

The potential-energy surface (PES) is defined as

$$\begin{aligned}U(Z_1, N_1, \beta_2, J, R_{\rm cont}) &= \Delta(Z_1, N_1) + \Delta(Z_2, N_2) \\ &+ V(Z_1, N_1, \beta_2, J, r = R_{\rm cont}) \\ &+ \tfrac{1}{2}C_1\left(\delta\beta_2^1\right)^2 + \tfrac{1}{2}C_2\left(\delta\beta_2^2\right)^2. \end{aligned} \quad (4)$$

In the DNS model, the nucleon transfer process takes place at the bottom of potential pocket, which is denoted as $R_{\rm cont}$. Here, $\Delta(Z_i, N_i)$ $(i = 1, 2)$ is mass excess of the fragment i, including the paring and shell corrections, which can be written as [78]

$$\begin{aligned}\Delta(Z_i, N_i) &= Z_i\Delta(^1H) + N_i\Delta(n) - a_{\rm v}(1 - \kappa I^2)A_i \\ &+ a_{\rm s}(1 - \kappa I^2)A_i^{2/3} + a_{\rm c}Z_i^2A_i^{-1/3} - c_4Z_i^2A_i^{-1} \\ &- E_{\rm pair}(Z_i, N_i) + E_{\rm sh}(Z_i, N_i). \end{aligned} \quad (5)$$

The liquid drop parameters can be seen in Ref. [78]. The pairing energy $E_{\rm pair}(Z_i, N_i) = E_{\rm pair}^0(Z_i, N_i)e^{-(E^*/a)^2}$. The shell correction energy $E_{\rm sh}(Z_i, N_i) = E_{\rm sh}^0(Z_i, N_i)e^{-E^*/E_{\rm d}}$. $E_{\rm d} = 5.48A_i^{1/3}/(1 + 1.3A_i^{-1/3})$ MeV. $a = A/12$ MeV^{-1}. $E_{\rm pair}^0$ is the pairing energy of the ground state, which is given by [78]

$$E_{\rm pair}^0 = \begin{cases} 2a_{\rm p}/A_i^{1/2}, & \text{for even } Z, \text{ even } N \text{ nuclei} \\ a_{\rm p}/A_i^{1/2}, & \text{for odd } A \text{ nuclei} \\ 0, & \text{for odd } Z, \text{ odd } N \text{ nuclei.} \end{cases} \quad (6)$$

Other liquid drop terms weakly depend on the fragment temperature.

The effective nucleus-nucleus interaction potential V can be written as

$$\begin{aligned}V(Z_1, N_1, \beta_2, J, r) &= V_{\rm N}(Z_1, N_1, \beta_2, r) \\ &+ V_{\rm C}(Z_1, N_1, \beta_2, r) + \frac{(J\hbar)^2}{2\zeta_{\rm rel}}. \end{aligned} \quad (7)$$

The detailed description of nuclear potential and Coulomb potential can be seen in Refs. [78,79].

C. Deexcitation process

The statistical approach is applied to deal with the deexcitation process. The Monte Carlo method is used to obtain the probabilities of all main possible decay channels. The decay chain is ended when fission happens or the fragments reach the ground state. In the ith deexcitation step the probability of the decay channel s can be written as

$$P_s(E_i^*) = \frac{\Gamma_s(E_i^*)}{\Gamma_{\rm tot}(E_i^*)}, \quad (8)$$

where s denotes different decay channels, such as neutron (n), proton (p), and α evaporation, γ emission, and fission (f). $\Gamma_{\rm tot} = \Gamma_n + \Gamma_p + \Gamma_\alpha + \Gamma_\gamma + \Gamma_{\rm f}$. E_i^* is the excitation energy before the ith decay step, which can be calculated from the equation $E_{i+1}^* = E_i^* - B_i$. B_i is the separation energy of particle or energy taken by the γ ray in the ith step. The partial decay widths of the excited nucleus for the evaporation of the light particle $\nu = (n, p, \alpha)$ can be estimated by using the Weisskopf-Ewing theory [80],

$$\Gamma_\nu(E^*, J) = \frac{(2s_\nu + 1)m_\nu}{\pi^2\hbar^2\rho(E^*, J)} \times \int_{I_\nu} \varepsilon\rho(E^* - B_\nu - \varepsilon, J)\sigma_{\rm inv}(\varepsilon)d\varepsilon, \quad (9)$$

where $I_\nu = [0, E^* - B_\nu]$ and $\sigma_{\rm inv}$ is the inverse reaction cross section for particle ν with channel energy ε. The Coulomb barrier for charged particle emission is calculated as shown in Ref. [81].

The fission decay width is usually calculated within the Bohr-Wheeler (BW) transition-state method [82]

$$\Gamma_{\rm f}(E^*, J) = \frac{1}{2\pi\rho_{\rm f}(E^*, J)} \times \int_{I_{\rm f}} \frac{\rho_{\rm f}(E^* - B_{\rm f} - \varepsilon, J)d\varepsilon}{1 + \exp[-2\pi(E^* - B_{\rm f} - \varepsilon)/\hbar\omega]}, \quad (10)$$

where $I_{\rm f} = [0, E^* - B_{\rm f}]$.

The γ emission width can be written as

$$\Gamma_\gamma(E^*, J) = \frac{3}{\rho(E^*, J)} \int_0^{E^*} \rho(E^* - \varepsilon, J)f_{E1}(\varepsilon)d\varepsilon. \quad (11)$$

Here, f_{E1} is the strength function, the detailed description of which can be seen in Ref. [83].

The level density is calculated as [20,84],

$$\rho(E^*, J) = K_{\rm coll}\frac{(2J + 1)\sqrt{a}}{24(E^* - \delta - E_{\rm rot})^2}\left(\frac{\hbar^2}{\zeta}\right)^{3/2} \times \exp[2\sqrt{a(E^* - \delta - E_{\rm rot})}], \quad (12)$$

where $E_{\rm rot} = \frac{\hbar^2 J(J+1)}{2\zeta}$. δ is the shift energy as shown in Eq. (6). $K_{\rm coll}$ is the collective enhancement factor [20].

III. RESULTS AND DISCUSSION

The PES of the reaction ^{48}Ca + ^{238}U is shown in the space of mass asymmetry and dynamical deformation in Fig. 1(a). The injection point for the initial configuration is denoted with a black solid circle. Figure 1(b) shows the driver potential as a function of mass asymmetry with $\beta_2 = 0$. In the concept of the DNS model, the CN is formed when the mass asymmetry of the DNS system overcomes the inner fusion barrier $B_{\rm fus}$, as shown in Fig. 1(b). And the sum of probabilities of fragments on the left side of the Businaro-Gallone (B.G.) point is considered as the fusion probability. Here, we extend the above definition to the case with dynamical deformation. The position (value of η) of the B.G. point as a function of β_2 is denoted with a wine line as shown in Fig. 1(a). In this work, we call this line the "B.G. line." For this case, the configurations on the left side of the B.G. line are considered as the occurrence of fusion.

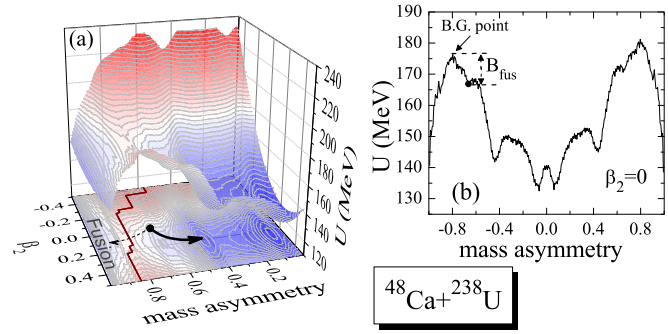

FIG. 1. (a) PES as a function of mass asymmetry η and β_2 for the reaction ^{48}Ca + ^{238}U. The wine line connects the B.G. points for different β_2. The injection point is denoted with the black solid circle. (b) Potential energy as a function of mass asymmetry with $\beta_2 = 0$ for the reaction ^{48}Ca + ^{238}U. The B.G. point and inner fusion barrier is denoted.

The code DNS-SYSU has been successfully used in investigating the MNT process for producing neutron-rich light, heavy, and superheavy nuclei. In this work, we apply the code in the FE process for synthesizing the SHN for the first time. To testify to the above extension of the fusion concept, we compare experimental data with the calculated results for synthesizing superheavy elements (SHEs) Cn in Fig. 2. Figure 2(a) compares the calculated capture cross sections with the experimental data. The calculated results are in good agreement with the experimental data. In Fig. 2(b) it can be seen that the fusion probability is very low and increases with the increasing incident energy. This is because the increase of incident energy enhances the probability of overcoming $B_{\rm fus}$.

We show the fusion probability for the reaction ^{48}Ca + ^{238}U as a function of $E_{\rm c.m.}$ and β_2 in Fig. 3(a). One interesting behavior is noticed that the occurrence of fusion mostly takes place for the case of β_2 with negative values, which means compact configuration enhances the fusion probability. It is consistent with the experimental results in Ref. [87]. This is because the inner fusion barriers $B_{\rm fus}$ for the negative values of β_2 are lower than that for the positive ones, as shown in Fig. 3(b). From $\beta_2 = -0.5$ to -0.4, the values of $B_{\rm fus}$ are even negative, which means η of the projectile-target configuration ($\eta = 0.6643$) is larger than η of the B.G. points of the corresponding β_2, as shown in Fig. 1(a). In Fig. 3(a), one also can see that, with increase of the incident energy, the peak of the curve moves to the right and gets close to the position $\beta_2 = 0$. This is because the high incident energy enhances the probability of overcoming the inner fusion barrier for the case of positive β_2 and weakens the relative inferior compared with the compact configuration.

The calculated evaporation residue (ER) cross sections in $3n$ and $4n$ evaporation channels are also compared with the experimental data in Fig. 2(c). Within the error bars, the calculations can reproduce the experimental data quite well. In Fig. 4, we further compare the calculated ER cross sections with the experimental data in the hot fusion reactions ^{48}Ca + ^{243}Am, ^{244}Pu, ^{248}Cm, and ^{249}Cf. Also, within the error

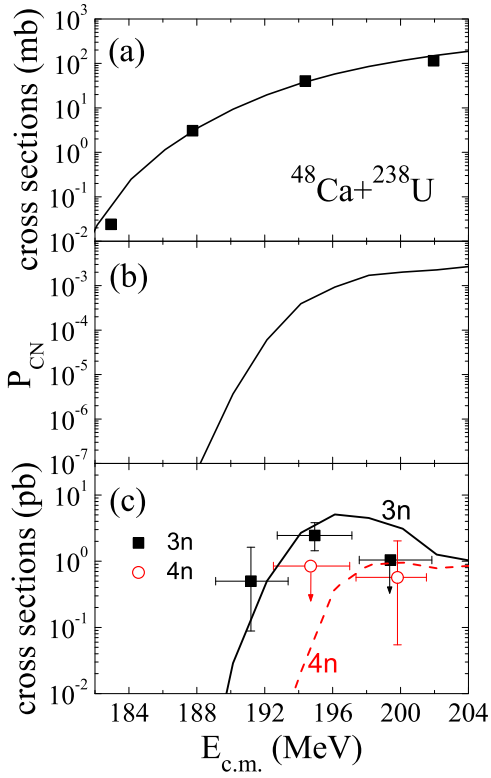

FIG. 2. (a) Comparison of calculated capture cross sections with experimental data [85] in the reaction $^{48}\mathrm{Ca}+{}^{238}\mathrm{U}$. (b) Calculated fusion probability as a function of incident energy within the DNS-SYSU code. The angular momentum is $J = 30\,\hbar$. (c) ER cross sections in the reaction $^{48}\mathrm{Ca}+{}^{238}\mathrm{U}$ for producing Cn isotopes. The experimental data [9] are denoted with circles and squares.

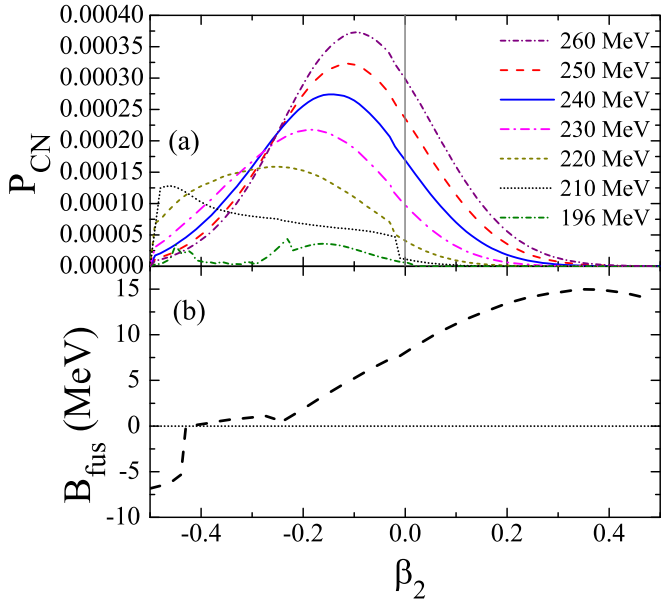

FIG. 3. (a) The fusion probability P_{CN} as a function of β_2 for the reaction $^{48}\mathrm{Ca}+{}^{238}\mathrm{U}$ at different incident energies. The angular momentum is $J = 30\,\hbar$. (b) The inner fusion barrier B_{fus} as a function of β_2. The horizontal dotted line denotes the $B_{\mathrm{fus}} = 0$.

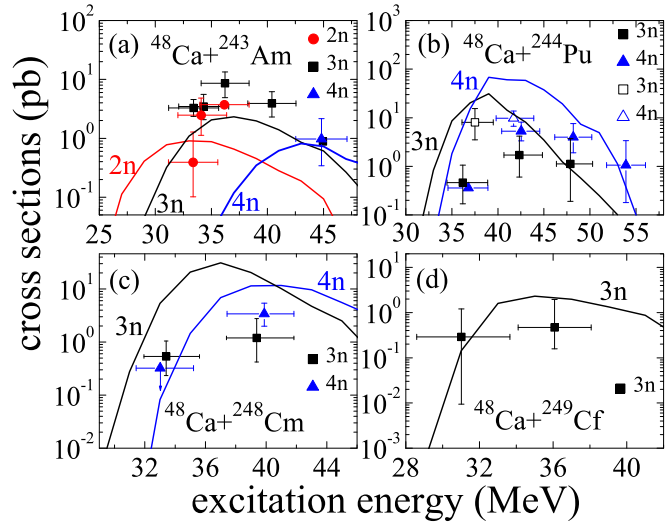

FIG. 4. Comparison of calculated ER cross sections with the available experimental data for the reactions $^{48}\mathrm{Ca}+{}^{243}\mathrm{Am}$ [11], ^{244}Pu [12,13], ^{248}Cm [14], and ^{249}Cf [15].

bars, the calculated results are in reasonably good agreement with the experimental data. It is demonstrated that the extension of the fusion concept in the DNS-SYSU code is reasonable.

On the other side, we show the production cross sections of isotopes produced in the MNT process. In the DNS concept, the diffusion process takes place at the bottom of potential pocket in the reaction systems with potential pockets. Figure 5(a) shows the mass distribution of primary fragments in the reaction $^{48}\mathrm{Ca}+{}^{238}\mathrm{U}$. For the case at $E_{\mathrm{c.m.}} = 180$ MeV, due to short interaction time, the main yields correspond to the initial configuration of $^{48}\mathrm{Ca}+{}^{238}\mathrm{U}$. With increasing incident energy, the yields of fragments far from the projectile and target increase strongly. Nevertheless, the production yields

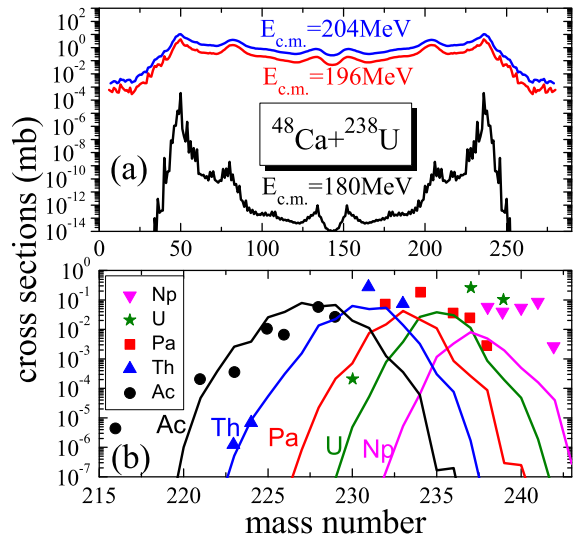

FIG. 5. (a) Mass distribution of primary fragments in the reaction $^{48}\mathrm{Ca}+{}^{238}\mathrm{U}$ at different incident energies. (b) Production cross sections of Ac, Th, Pa, U, and Np isotopes in the reaction $^{48}\mathrm{Ca}+{}^{238}\mathrm{U}$ at $E_{\mathrm{c.m.}} = 196$ MeV. The experimental data are from Ref. [86].

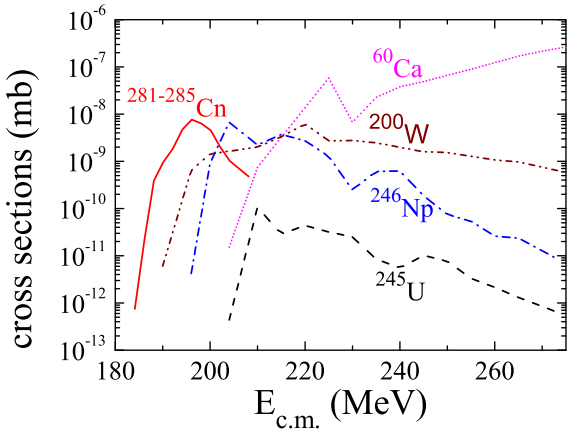

FIG. 6. Cross sections as a function of incident energy for producing SHN $^{281-285}$Cn and neutron rich unknown isotopes ^{60}Ca, ^{200}W, ^{245}U, and ^{246}Np in the reaction ^{48}Ca + ^{238}U.

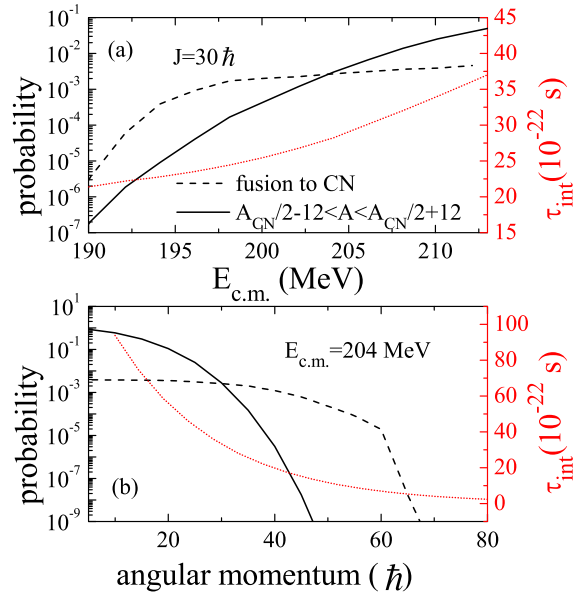

FIG. 7. The probabilities of compound nucleus formation and production of symmetry fragments with $(A_{CN}/2 - 12) < A < (A_{CN}/2 + 12)$ as a function of incident energy with angular momentum $J = 30\hbar$ (a) and entrance angular momentum at $E_{c.m.} = 204$ MeV (b) in the reaction ^{48}Ca + ^{238}U. The red dotted lines denote the interaction time of diffusion process, which corresponds to the vertical axis on the right side.

around the ^{48}Ca and ^{238}U still show advantages. In Fig. 5(b), we show the comparison of calculated production cross sections of target-like products in the reaction ^{48}Ca + ^{238}U with the experimental data. One can see that the calculated results are in good agreement with the experimental data. The FE and MNT processes can be simultaneously and reasonably described for the reaction ^{48}Ca + ^{238}U within the code of DNS-SYSU. Note that parameters in the DNS-SYSU code are fixed not only in this work but also in the previous related works. To compare the production of isotopes through the two processes in the collisions ^{48}Ca + ^{238}U, Fig. 6 shows the total ER cross sections for producing Cn isotopes in the FE process, and the exotic, unknown, neutron-rich isotopes could be produced in the MNT process. It is shown that the total ER cross section for synthesizing $^{281-285}$Cn strongly depends on the incident energy. The maximal ER cross section is about 8 pb at $E_{c.m.} = 196$ MeV. In the low-incident-energy region, the increase of the ER cross section with increasing incident energy is mainly due to the increase of capture cross section and the fusion probability. For SHN, the fission probability is very high and increases intensively with the increasing excitation energy, which results in the strong decrease of the ER cross section with the incident energy above $E_{c.m.} = 196$ MeV. For target-like products ^{246}Np and ^{245}U produced in the MNT process, the optimal incident energies are larger than that for producing Cn isotopes in the FE process. Still, due to the influence of fission, it is noticed that the yield distribution of final fragments increases at first and then decreases with increasing incident energy. However, for producing isotopes ^{60}Ca near the neutron drip line, the behavior of relatively weak energy dependence is noticed when the yields reach a relatively high value. We also show the result for producing the neutron-rich isotope ^{200}W with $N = 126$. Still, the relatively weak energy dependence is noticed. Obviously, the optimal incident energy for producing SHN in FE process is lower than that in the MNT process for producing neutron-rich isotopes.

As shown in Fig. 1, the DNS could overcome the fusion barrier to form the CN or slide into the valley and evolve towards the symmetry configurations. To further clarify the competitions between two processes, Fig. 7(a) shows the probabilities of fusion and production of fragments in the near symmetry mass region in the MNT process as a function of incident energy. The entrance angular momentum is fixed at $J = 30\hbar$. One can see that the fusion probability is higher than that for producing fragments with $(A_{CN}/2 - 12) < A < (A_{CN}/2 + 12)$ at the low-incident-energy region. With the increase of incident energy, the fusion probability increase strongly. Then, the behavior of weak energy dependence is noticed after reaching a relative high level of probability. The above behaviors for fusion probability are due to the role of the inner fusion barrier. On the other hand, because of the tendency to minimize the potential energy, for producing near symmetry configuration fragments, the probability continuously increases and exceeds the fusion probability in the high-incident-energy region, although the near symmetry fragments are far from the ^{48}Ca + ^{238}U configuration. The dissipated excitation energy of the DNS is related to the contact time. We also show the contact time in the diffusion process. It can be seen that the high incident energy enhances the contact time and then enhances the probabilities of fusion and fragments far from the initial configuration. The variation of probabilities with the entrance angular momentum is shown in Fig. 7(b). For both the fusion and formation of the near symmetry configuration, the probabilities decrease with increasing angular momentum, which is because the centrifugal potential affects the suppression of interaction time. The great advantage of probability in fusion is noticed for the cases of $J > 30\hbar$. Furthermore, the less intense variation of fusion probability is noticed.

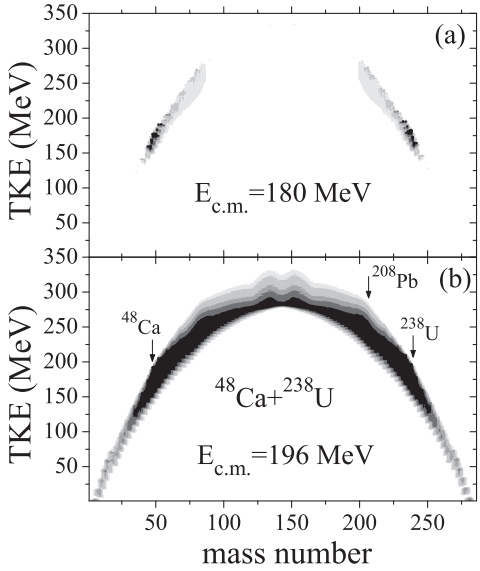

FIG. 8. TKE-mass distributions of MNT products in the reaction $^{48}\mathrm{Ca}+^{238}\mathrm{U}$ at (a) $E_{\mathrm{c.m.}}=180$ and (b) 196 MeV, respectively.

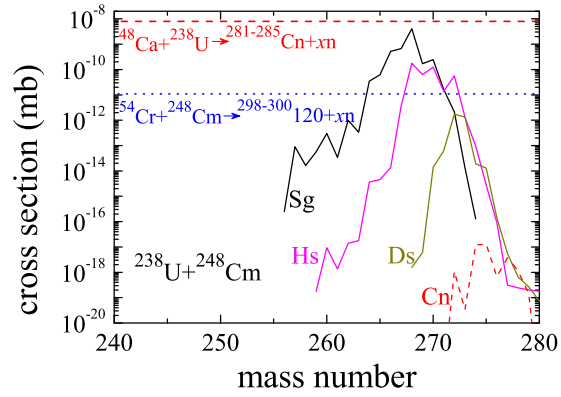

FIG. 9. Cross sections for producing SHN in MNT reaction $^{238}\mathrm{U}+^{248}\mathrm{Cm}$ ($E_{\mathrm{c.m.}}=800$ MeV). The horizontal dashed and dotted lines denote a maximal synthesis cross section of $^{281-285}$Cn and $^{298-300}120$ in FE reaction $^{48}\mathrm{Ca}+^{238}\mathrm{U}$ and $^{54}\mathrm{Cr}+^{248}\mathrm{Cm}$, respectively.

Figure 8 shows the calculated correlations of total kinetic energy and the mass distribution of primary products produced in MNT process in the reaction $^{48}\mathrm{Ca}+^{238}\mathrm{U}$ at $E_{\mathrm{c.m.}}=180$ and 196 MeV. One can see that most events are located at the configurations around $^{48}\mathrm{Ca}+^{238}\mathrm{U}$, especially for $E_{\mathrm{c.m.}}=180$ MeV. In Fig. 8(a), almost no symmetry fragments are produced. The distribution of the fragments is wide for $E_{\mathrm{c.m.}}=196$ MeV, as shown in Fig. 8(b). One can see that, besides the ^{48}Ca and ^{238}U combination, the large yield of fragments in the region of the doubly magic nucleus ^{208}Pb (and the complimentary light fragments) is a pronounced feature of the TKE-mass distribution. As shown in Fig. 1, due to shell closures, deep valleys are shown around $A=208$ ($N=126$ and $Z=82$) and around the complimentary light fragment $A=78$. A similar behavior was also shown based on a Langevin-type approach [46].

To compare the FE and MNT processes for producing SHN, we show the production cross sections of SHN in the MNT reaction $^{238}\mathrm{U}+^{248}\mathrm{Cm}$ at $E_{\mathrm{c.m.}}=800$ MeV and maximal ER cross sections for the synthesis of $^{281-285}$Cn in the reaction $^{48}\mathrm{Ca}+^{238}\mathrm{U}\rightarrow{}^{281-285}\mathrm{Cn}+xn$ in Fig. 9. The maximal cross section for producing $^{281-285}$Cn in the reaction $^{48}\mathrm{Ca}+^{238}\mathrm{U}$ is 8 pb, which corresponds to $E_{\mathrm{c.m.}}=196$ MeV. We denote the 8 pb with a horizontal dashed line. For producing the same element Cn, the cross section in the MNT reaction $^{238}\mathrm{U}+^{248}\mathrm{Cm}$ is several orders of magnitude lower than that in the fusion reaction $^{48}\mathrm{Ca}+^{238}\mathrm{U}$. Although collisions with heavier projectiles and targets could enhance the production yields of superheavy nuclei in the MNT process [70], the limited amount of target atoms and low beam intensity of projectiles make the performance of the experiments quite difficult. We also show the cross section of $\mathrm{Cr}+^{248}\mathrm{Cm}$. It can be seen that the cross section is close 0.01 pb. However, the production cross section of the $Z=120$ isotopes in $^{238}\mathrm{U}+^{248}\mathrm{Cm}$ is below 10^{-11} pb, which cannot be reached in laboratories. Therefore, the FE approach is the only approach for synthesizing new elements.

IV. CONCLUSIONS

The FE reactions has been extensively used in the synthesis of SHN. Also, the MNT process was proposed as one alternative approach for producing SHN, especially the neutron-rich ones. To investigate and compare the FE and MNT processes and make more reliable predictions for producing SHN, the unified description of these processes is performed in the reaction $^{48}\mathrm{Ca}+^{238}\mathrm{U}$ within the DNS model. With the reasonable extension of the fusion concept, the model can reproduce the experimental evaporation residue cross sections quite well in the reactions $^{48}\mathrm{Ca}+^{238}\mathrm{U}$, ^{243}Am, ^{244}Pu, ^{248}Cm, ^{249}Cf. It is noticed that the DNS-SYSU model can simultaneously well describe the FE and MNT processes. The behavior of fusion probability with the dynamical deformation in this work supports the experimental result [87] that the compact configuration enhances fusion probability.

We compare the production cross sections of SHN in fusion reactions $^{48}\mathrm{Ca}+^{238}\mathrm{U}$ and $^{54}\mathrm{Cr}+^{248}\mathrm{Cm}$ with the MNT reaction $^{238}\mathrm{U}+^{248}\mathrm{Cm}$. It can be seen that the collisions of $^{238}\mathrm{U}+^{248}\mathrm{Cm}$ can generate plenty of superheavy isotopes. However, the production cross section decreases strongly with increasing charge number of objective products. For producing isotopes of Cn and the SHE with $Z=120$, the FE reactions show great advantages of cross sections over the MNT reaction $^{238}\mathrm{U}+^{248}\mathrm{Cm}$. The stable beam-induced fusion reactions are still the favorable approach for producing SHN and is the only approach to synthesize the SHE beyond oganesson. However, for producing neutron-rich SHN, even nuclei on the "island of stability" reactions using MNT could be considerable an alternative.

ACKNOWLEDGMENT

This work was supported by the National Natural Science Foundation of China under Grants No. 12075327 and No. 11805015.

[1] Yu. Ts. Oganessian and V. K. Utyonkov, Rep. Prog. Phys. **78**, 036301 (2015).
[2] V. V. Volkov, Phys. Rep. **44**, 93 (1978).
[3] G. G. Adamian, N. V. Antonenko, A. Diaz-Torres, and S. Heinz, Eur. Phys. J. A **56**, 47 (2020).
[4] F. S. Zhang, C. Li, L. Zhu, and P. W. Wen, Front. Phys. **13**, 132113 (2018).
[5] L. Zhu, C. Li, C. C. Guo, J. Su, P. W. Wen, G. Zhang, and F. S. Zhang, Int. J. Mod. Phys. E **29**, 2030004 (2020).
[6] W. Loveland, Front. Phys. **7**, 23 (2019).
[7] S. Hofmann and G. Münzenberg, Rev. Mod. Phys. **72**, 733 (2000); S. Hofmann, F. P. Heßberger, D. Ackermann, G. Münzenberg, S. Antalic, P. Cagarda, B. Kindler, J. Kojouharova, M. Leino, B. Lommel, R. Mann, A. G. Popeko, S. Reshitko, S. Śaro, J. Uusitalo, and A. V. Yeremin, Eur. Phys. J. A **14**, 147 (2002).
[8] K. Morita, K. Morimoto, D. Kaji, H. Haba, K. Ozeki, Y. Kudou, T. Sumita, Y. Wakabayashi, A. Yoneda, K. Tanaka, S. Yamaki, R. Sakai, T. Akiyama, S. Goto, H. Hasebe, M. Huang, T. Huang, E. Ideguchi, Y. Kasamatsu, K. Katori *et al.*, J. Phys. Soc. Jpn. **81**, 103201 (2012).
[9] Yu. Ts. Oganessian, F. S. Abdullin, P. D. Bailey, D. E. Benker, M. E. Bennett, S. N. Dmitriev, J. G. Ezold, J. H. Hamilton, R. A. Henderson, M. G. Itkis *et al.*, Phys. Rev. Lett. **104**, 142502 (2010).
[10] Yu. Ts. Oganessian, J. Phys. G **34**, R165 (2007).
[11] Yu. Ts. Oganessian, F. Sh. Abdullin, S. N. Dmitriev, J. M. Gostic, J. H. Hamilton, R. A. Henderson, M. G. Itkis, K. J. Moody, A. N. Polyakov, A. V. Ramayya, J. B. Roberto, K. P. Rykaczewski, R. N. Sagaidak, D. A. Shaughnessy, I. V. Shirokovsky, M. A. Stoyer, N. J. Stoyer, V. G. Subbotin, A. M. Sukhov, Yu. S. Tsyganov, V. K. Utyonkov, A. A. Voinov, and G. K. Vostokin, Phys. Rev. C **87**, 014302 (2013).
[12] Yu. Ts. Oganessian, V. K. Utyonkov, Yu. V. Lobanov, F. Sh. Abdullin, A. N. Polyakov, I. V. Shirokovsky *et al.*, Phys. Rev. C **69**, 054607 (2004).
[13] Ch. E. Düllmann, M. Schädel, A. Yakushev, A. Türler, K. Eberhardt, J. V. Kratz *et al.*, Phys. Rev. Lett. **104**, 252701 (2010).
[14] Yu. Ts. Oganessian, V. K. Utyonkov, Yu. V. Lobanov, F. Sh. Abdullin, A. N. Polyakov, I. V. Shirokovsky *et al.*, Phys. Rev. C **70**, 064609 (2004).
[15] Yu. Ts. Oganessian, V. K. Utyonkov, Yu. V. Lobanov, F. Sh. Abdullin, A. N. Polyakov, R. N. Sagaidak *et al.*, Phys. Rev. C **74**, 044602 (2006).
[16] S. A. Giuliani, Z. Matheson, W. Nazarewicz, E. Olsen, P. G. Reinhard, J. Sadhukhan, B. Schuetrumpf, N. Schunck, and P. Schwerdtfeger, Rev. Mod. Phys. **91**, 011001 (2019).
[17] A. K. Nasirov, G. Mandaglio, G. Giardina, A. Sobiczewski, and A. I. Muminov, Phys. Rev. C **84**, 044612 (2011).
[18] Z. H. Liu and J. D. Bao, Phys. Rev. C **87**, 034616 (2013).
[19] S. Hofmann, J. Phys. G **42**, 114001 (2015).
[20] V. I. Zagrebaev and W. Greiner, Nucl. Phys. A **944**, 257 (2015).
[21] C. E. Düllmann, EPJ Web Conf. **131**, 08004 (2016).
[22] G. G. Adamian, N. V. Antonenko, and H. Lenske, Nucl. Phys. A **970**, 22 (2018).
[23] L. Zhu, W. J. Xie, and F. S. Zhang, Phys. Rev. C **89**, 024615 (2014).
[24] F. Li, L. Zhu, Z. H. Wu, X. B. Yu, J. Su, and C. C. Guo, Phys. Rev. C **98**, 014618 (2018).
[25] K. V. Novikov, E. M. Kozulin, G. N. Knyazheva, I. M. Itkis, M. G. Itkis, A. A. Bogachev *et al.*, Phys. Rev. C **102**, 044605 (2020).
[26] Y. T. Oganessian, V. K. Utyonkov, Y. V. Lobanov, F. S. Abdullin, A. N. Polyakov, R. N. Sagaidak, I. V. Shirokovsky, Y. S. Tsyganov, A. A. Voinov, A. N. Mezentsev *et al.*, Phys. Rev. C **79**, 024603 (2009).
[27] S. Hofmann, S. Heinz, R. Mann, J. Maurer, G. Münzenberg, S. Antalic, W. Barth, H. G. Burkhard, L. Dahl, K. Eberhardt *et al.*, Eur. Phys. J. A **52**, 180 (2016).
[28] V. Zagrebaev and W. Greiner, Phys. Rev. Lett. **101**, 122701 (2008).
[29] Y. X. Watanabe, Y. H. Kim, S. C. Jeong, Y. Hirayama, N. Imai, H. Ishiyama, H. S. Jung, H. Miyatake, S. Choi, J. S. Song, E. Clement, G. de France, A. Navin, M. Rejmund, C. Schmitt, G. Pollarolo, L. Corradi, E. Fioretto, D. Montanari, M. Niikura *et al.*, Phys. Rev. Lett. **115**, 172503 (2015).
[30] S. Wuenschel, K. Hagel, M. Barbui, J. Gauthier, X. G. Cao, R. Wada, E. J. Kim, Z. Majka, R. Planeta, Z. Sosin, A. Wieloch, K. Zelga, S. Kowalski, K. Schmidt, C. Ma, G. Zhang, and J. B. Natowitz, Phys. Rev. C **97**, 064602 (2018).
[31] V. I. Zagrebaev, Yu. Ts. Oganessian, M. G. Itkis, and W. Greiner, Phys. Rev. C **73**, 031602(R) (2006).
[32] M. R. Pahlavani and M. M. Dinan, Phys. Rev. C **103**, 034608 (2021).
[33] V. L. Litnevsky, F. A. Ivanyuk, G. I. Kosenko, and S. Chiba, Phys. Rev. C **101**, 064616 (2020).
[34] K. Sekizawa and K. Hagino, Phys. Rev. C **99**, 051602(R) (2019).
[35] A. S. Umar, V. E. Oberacker, and C. Simenel, Phys. Rev. C **94**, 024605 (2016).
[36] C. Yu and L. Guo, Sci. China: Phys., Mech. Astron. **60**, 092011 (2017).
[37] Z.-H. Liu and J.-D. Bao, Phys. Rev. C **89**, 024604 (2014).
[38] C. Shen, Y. Abe, D. Boilley, G. Kosenko, and E. Zhao, Int. J. Mod. Phys. E **17**, 66 (2008).
[39] C. Shen, G. Kosenko, and Y. Abe, Phys. Rev. C **66**, 061602(R) (2002).
[40] V. I. Zagrebaev, Phys. Rev. C **64**, 034606 (2001).
[41] K. Siwek-Wilczyńska, T. Cap, M. Kowal, A. Sobiczewski, and J. Wilczyński, Phys. Rev. C **86**, 014611 (2012).
[42] V. L. Litnevsky, V. V. Pashkevich, G. I. Kosenko, and F. A. Ivanyuk, Phys. Rev. C **89**, 034626 (2014).
[43] G. G. Adamian, N. V. Antonenko, H. Lenske, and L. A. Malov, Phys. Rev. C **101**, 034301 (2020).
[44] A. V. Karpov and V. V. Saiko, Phys. Rev. C **96**, 024618 (2017).
[45] K. Sekizawa, Front. Phys. **7**, 00020 (2019).
[46] V. Zagrebaev and W. Greiner, J. Phys. G: Nucl. Part. Phys. **34**, 1 (2007).
[47] X. Jiang and N. Wang, Phys. Rev. C **101**, 014604 (2020).
[48] Z. Wu and L. Guo, Phys. Rev. C **100**, 014612 (2019).
[49] A. Winther, Nucl. Phys. A **572**, 191 (1994).
[50] P. W. Wen, C. Li, L. Zhu, C. Lin, and F. S. Zhang, J. Phys. G **44**, 115101 (2017).
[51] P. W. Wen, A. K. Nasirov, C. J. Lin, and H. M. Jia, J. Phys. G **47**, 075106 (2020).
[52] K. Zhao, Z. Liu, F. S. Zhang, and N. Wang, Phys. Lett. B **815**, 136101 (2021).
[53] C. Li, J. Tian, and F. S. Zhang, Phys. Lett. B **809**, 135697 (2020).

[54] C. Li, P. Wen, J. Li, G. Zhang, B. Li, X. Xu, Z. Liu, S. Zhu, and F. S. Zhang, Phys. Lett. B **776**, 278 (2018).
[55] J. Hong, G. G. Adamian, N. V. Antonenko, P. Jachimowicz, and M. Kowal, Phys. Rev. C **103**, L041601 (2021).
[56] X. J. Bao, Y. Gao, J. Q. Li, and H. F. Zhang, Phys. Rev. C **92**, 034612 (2015).
[57] X. J. Bao, Y. Gao, J. Q. Li, and H. F. Zhang, Phys. Rev. C **91**, 011603(R) (2015).
[58] L. Zhu, Z. Q. Feng, C. Li, and F. S. Zhang, Phys. Rev. C **90**, 014612 (2014).
[59] Z. H. Wu, L. Zhu, F. Li, X. B. Yu, J. Su, and C. C. Guo, Phys. Rev. C **97**, 064609 (2018).
[60] Z. Q. Feng, G. M. Jin, and J. Q. Li, Nucl. Phys. A **836**, 82 (2010).
[61] L. Zhu, C. Li, J. Su, C. C. Guo, and W. Hua, Phys. Lett. B **791**, 20 (2019).
[62] L. Zhu, J. Su, W. J. Xie, and F. S. Zhang, Phys. Lett. B **767**, 437 (2017).
[63] L. Zhu, Phys. Lett. B **816**, 136226 (2021).
[64] G. Zhang, C. A. T. Sokhna, Z. Liu, and F. S. Zhang, Phys. Rev. C **100**, 024613 (2019).
[65] X. J. Bao, Phys. Rev. C **102**, 054613 (2020).
[66] Z. Cheng and X. J. Bao, Phys. Rev. C **103**, 024613 (2021).
[67] G. G. Adamian, N. V. Antonenko, and D. Lacroix, Phys. Rev. C **82**, 064611 (2010).
[68] S. Q. Guo, X. J. Bao, H. F. Zhang, J. Q. Li, and N. Wang, Phys. Rev. C **100**, 054616 (2019).
[69] Yu. E. Penionzhkevich, G. G. Adamian, and N. V. Antonenko, Phys. Lett. B **621**, 119 (2005).
[70] L. Zhu, Chin. Phys. C **43**, 124103 (2019).
[71] J. Q. Li and G. Wolschin, Phys. Rev. C **27**, 590 (1983).
[72] G. Wolschin and W. Nörenberg, Z. Phys. A: At. Nucl. (1975) **284**, 209 (1978).
[73] B. Wang, K. Wen, W. J. Zhao, E. G. Zhao, and S. G. Zhou, At. Data Nucl. Data Tables **114**, 281 (2017).
[74] L. Zhu, J. Su, P. W. Wen, C. C. Guo, and C. Li, Phys. Rev. C **98**, 034609 (2018).
[75] W. D. Myers and W. J. Swiatecki, Nucl. Phys. **81**, 1 (1966).
[76] W. Nörenberg, Z. Phys. A **274**, 241 (1975).
[77] S. Ayik, B. Schürmann, and W. Nörenberg, Z. Phys. A: At. Nucl. (1975) **277**, 299 (1976).
[78] L. Zhu, P. W. Wen, C. J. Lin, X. J. Bao, J. Su, C. Li, and C. C. Guo, Phys. Rev. C **97**, 044614 (2018).
[79] C. Y. Wong, Phys. Rev. Lett. **31**, 766 (1973).
[80] V. F. Weisskopf and D. H. Ewing, Phys. Rev. **57**, 472 (1940).
[81] A. S. Zubov, G. G. Adamian, N. V. Antonenko, S. P. Ivanova, and W. Scheid, Phys. Rev. C **68**, 014616 (2003).
[82] N. Bohr and J. A. Wheeler, Phys. Rev. **56**, 426 (1939).
[83] L. Zhu, J. Phys. G **47**, 065107 (2020).
[84] A. V. Ignatyuk, K. K. Istekov, and G. N. Smirenkin, Sov. J. Nucl. Phys. **29**, 450 (1979).
[85] M. G. Itkis *et al.*, J. Nucl. Radiochem. Sci. **3**, 57 (2002).
[86] H. M. Devaraja, S. Heinz, D. Ackermann, T. Göbel, F. P. Heßberger, S. Hofmann, J. Maurer, G. Münzenberg, A. G. Popeko, and A. V. Yeremin, Eur. Phys. J. A **56**, 224 (2020).
[87] K. Nishio, H. Ikezoe, S. Mitsuoka, I. Nishinaka, Y. Nagame, Y. Watanabe, T. Ohtsuki, K. Hirose, and S. Hofmann, Phys. Rev. C **77**, 064607 (2008).